J. Phys.: Condens. Matter 4 (1992) 375–388. Printed in the UK

Ferroelastic phase transition in the sanmartinite ($ZnWO_4$)–cuproscheelite ($CuWO_4$) solid solution

Paul F Schofield† and Simon A T Redfern†‡

† Department of Geology, University of Manchester, Oxford Road, Manchester M13 9PL, UK

‡ Department of Chemistry, University of Manchester, Oxford Road, Manchester M13 9PL, UK

Received 10 September 1991

Abstract. Tungstates in the composition range $ZnWO_4$–$CuWO_4$ (sanmartinite–cuproscheelite) have been synthesized. Complete solid solution between the end members is found for samples annealed at 600 °C. The lattice parameters across the solid solution vary continuously and reveal a structural phase transition between the $P2/c$ sanmartinite structure and $P\bar{1}$ cuproscheelite structure at around $Zn_{0.78}Cu_{0.22}WO_4$. The spontaneous strain arising in the triclinic phase is large, amounting to some 6.5% in the cuproscheelite end member, and has been used as a measure of the order parameter for the transition. The structural phase transition is potentially ferroelastic and appears continuous as a function of composition at room temperature and pressure. The transition is successfully modelled in terms of a second-order Landau-type phenomenological potential.

1. Introduction

Sanmartinite ($ZnWO_4$) and cuproscheelite ($CuWO_4$) are two members of a large family of structurally related divalent transition metal tungstates with small cations, of the general form AWO_4 (A = Zn,Mg,Mn,Fe,Co,Ni,Cd,Cu). These tungstates all have the basic wolframite structure, and sometimes are also referred to as $NiWO_4$-type tungstates.

Single crystals of zinc tungstate have, in particluar, received much attention because of their potential technological significance in applications such as scintillation detectors, photoanodes, and masers. With these applications in mind, studies of a wide range properties such as crystal growth (Van Uitert *et al* 1963, Földvári *et al* 1986, Arora *et al* 1988, Földvári *et al* 1989), electrical characteristics (Bharati *et al* 1980, Arora and Matthew 1989), elastic and acoustic properties (Pisorevskii *et al* 1988), optical properties (Scott 1968, Arora *et al* 1989), reduction studies (Basu and Sale 1978, 1979), defect characteristics (e.g. Watterich *et al* 1991), as well as structural studies (e.g. Filipenko *et al* 1968), abound in the literature and are too diverse to review thoroughly here. Although a vast literature is devoted to studies of the pure and near-pure end member phases of this family of tungstates, there has been minimal consideration of possible solid-state series between these phases. Šroubek and Žďánský (1966) studied the defect properties of small concentrations (ppm) of Cu^{2+} paramagnetic impurity ions and investigated the site symmetry. No

0953-8984/92/020375 + 14 $04.50

further consideration has been given, however, to the effects of large concentrations of Cu^{2+} on the structure. In contrast, our particular concern here centres on the effect of substitution of up to 100% Cu^{2+} for Zn^{2+} into the $ZnWO_4$ structure to form the previously unreported solid solution series $(Cu_xZn_{1-x})WO_4$, and we analyse an associated potentially ferroelastic structural phase transition within a Landau-type model.

2. Crystal structure of the end members

The structure of $ZnWO_4$ was first refined by Filipenko *et al* (1968) who reported it isostructural with the group of $NiWO_4$-type monoclinic wolframite phases. The wolframite structure has been extensively studied by diffraction methods (Broch 1929, Keeling 1957, Chicagov *et al* 1966, Dachs *et al* 1967, Ülku 1967, Cid-dresdner and Escobar 1968, Sleight 1972) and refined in space group $P2/c$ (C_{2h}^4) with two formula units per unit cell. The structure comprises infinite zigzag chains running parallel to [001] and formed entirely of either edge-sharing ZnO_6 octahedra or edge-sharing WO_6 octahedra. Each chain of ZnO_6 octahedra is corner-linked to four chains of WO_6 octahedra, and vice versa, leaving open channels parallel to the z-axis (figure 1). The point symmetry of both the W and Zn sites is C_2 with three pairwise equivalent bonds in each octahedron. Zn–O bond lengths lie between 2.06 Å and 2.14 Å.

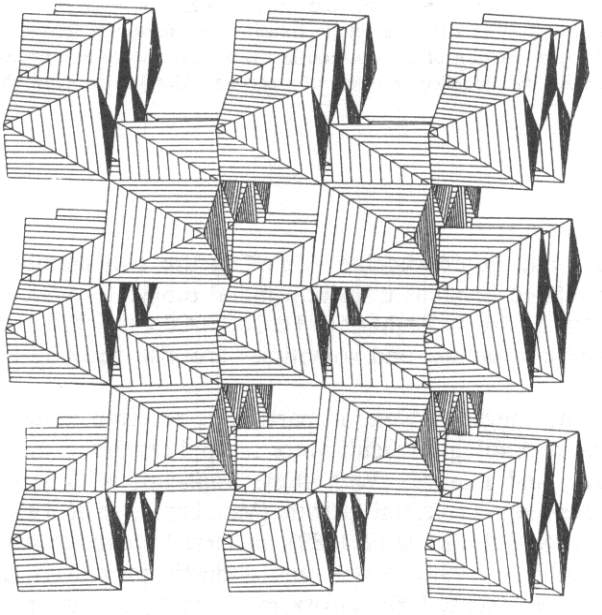

Figure 1. Structure of $ZnWO_4$ showing the zigzag corner-linked chains of ZnO_6 and WO_6 running away from the viewer (into the page). The y-axis is horizontal, the x-axis vertical. Nine WO_6 octahedral chains are shown corner-linked to four ZnO_6 octahedral chains.

The structure of $CuWO_4$ was solved in 1970 by Kihlborg and Gebert and later by Von Klein and Weitzel (1975) and is topologically identical to that of $ZnWO_4$. It is, however, distorted with respect to monoclinic wolframite structure to the lower

symmetry space group $P\bar{1}$. The chains composed of CuO_6 octahedra are distorted by the Cu coordination requirements which reduce the divalent cation site symmetry to $\bar{1}$. The Jahn–Teller effect on the Cu^{2+} removes the degeneracy of the 3d orbitals and results in the lengthening of two opposite Cu–O bonds within an elongated octahedron, with Cu surrounded in approximately square planar configuration by four oxygens at a distance of approximately 1.98 (± 0.02) Å and two at a longer distance of about 2.4 Å (Kihlborg and Gilbert 1970). In contrast WO_6 octahedra are only slightly distorted, but the tungsten atom is located offcentre. The overall effect is to destroy the monoclinic symmetry with α and γ deviating significantly from 90°.

We now report on investigations into the structural characteristics of tungstates in the composition range $(Cu_xZn_{1-x})WO_4$.

3. Synthesis and experimental analysis

Samples were synthesized at 5 mol% intervals across the composition range from $ZnWO_4$ to $CuWO_4$ using a direct precipitation method, frequently employed for the synthesis of molybdate and tungstate end members (Sleight 1972) and successfully used for the synthesis of the $Ca(W_xMo_{1-x})O_4$ solid solution (Shoji and Sasaki 1978, Tyson *et al* 1988).

Table 1. Unit cell edge dimensions (Å), unit cell angles (deg) and unit cell volume (Å^3) for all synthetic samples

mol% $ZnWO_4$	a	b	c	α	β	γ	V
0	4.7046(5)	5.8392(6)	4.8815(3)	91.669(8)	92.504(8)	82.812(8)	132.88(1)
5	4.7060(2)	5.8398(2)	4.8824(2)	91.615(3)	92.450(3)	82.905(3)	132.994(6)
10	4.7059(4)	5.8380(8)	4.8803(5)	91.591(8)	92.48(1)	82.889(9)	132.89(2)
15	4.7038(2)	5.8337(4)	4.8819(3)	91.557(5)	92.343(5)	82.124(6)	132.853(9)
20	4.7020(3)	5.8305(5)	4.8837(3)	91.500(6)	92.281(6)	83.300(7)	132.83(1)
25	4.7023(3)	5.8280(3)	4.8835(2)	91.471(5)	92.275(5)	83.383(6)	132.806(9)
30	4.6976(5)	5.8190(8)	4.8879(4)	91.302(7)	92.075(8)	83.94(1)	132.75(2)
35	4.6976(4)	5.8151(6)	4.8875(3)	91.311(6)	92.021(7)	84.023(8)	132.68(2)
40	4.6937(4)	5.8007(6)	4.8917(7)	91.145(7)	91.814(8)	84.636(8)	132.52(1)
45	4.6918(6)	5.7958(6)	4.8896(5)	91.075(8)	91.77(1)	84.75(1)	132.32(2)
50	4.6918(6)	5.7889(6)	4.8945(6)	90.97(1)	91.70(1)	85.23(1)	132.40(2)
55	4.6890(4)	5.7793(7)	4.8998(3)	90.825(6)	91.480(8)	85.89(1)	132.38(1)
60	4.6890(2)	5.7738(3)	4.9000(2)	90.804(4)	91.469(4)	86.022(5)	132.287(8)
65	4.6861(2)	5.7608(3)	4.9033(2)	90.640(4)	91.334(5)	86.710(5)	132.109(8)
70	4.6823(2)	5.7435(3)	4.9065(2)	90.421(4)	91.172(4)	87.833(4)	131.825(7)
75	4.6837(3)	5.7406(5)	4.9115(3)	90.293(6)	91.115(6)	88.383(7)	131.97(1)
80	4.6846(2)	5.7318(3)	4.9158(3)	90.0	90.981(5)	90.0	131.974(8)
85	4.6865(3)	5.7258(3)	4.9197(3)	90.0	90.841(5)	90.0	132.001(8)
90	4.6880(2)	5.7217(3)	4.9224(2)	90.0	90.734(4)	90.0	132.026(7)
95	4.6882(3)	5.7222(3)	4.9230(3)	90.0	90.742(5)	90.0	132.058(9)
100	4.6913(3)	5.7199(3)	4.9271(3)	90.0	90.615(5)	90.0	132.205(9)

Analytical grade reagents $ZnSO_4 \cdot 7H_2O$ and $CuSO_4 \cdot 5H_2O$ were stoichiometrically mixed and dissolved in 250 ml of deionized water according to the equations:

$$ZnSO_4 \cdot 7H_2O_{(aq)} + Na_2WO_4 \cdot 2H_2O_{(aq)} \Rightarrow ZnWO_{4(S)} + Na_2SO_{4(aq)} + 9H_2O$$

and

$$CuSO_4 \cdot 5H_2O_{(aq)} + Na_2WO_4 \cdot 2H_2O_{(aq)} \Rightarrow CuWO_{4(S)} + Na_2SO_{4(aq)} + 7H_2O.$$

Whilst this solution was boiling, 250 ml of solution containing a stoichiometric amount of $Na_2WO_4 \cdot 2H_2O$ was added. A blue/green precipitate appeared instantly and was allowed to settle before being separated from the remaining solution. After thorough washing and drying the precipitate was ground by hand in an agate pestle and mortar and annealed, under atmospheric conditions, in a muffle furnace at 600 °C for 88 h.

The dissociation of $ZnSO_4$ is significantly less than that of $CuSO_4$; thus it may be expected that, under equilibrium conditions, the first precipitate to appear would be Cu-rich whilst the final precipitate would be Zn-rich. This effect is in fact very small, however, because the activities of Cu^{2+} and Zn^{2+} in the Na_2WO_4 solution are very low and the measured $Cu^{2+}/(Cu^{2+} + Zn^{2+})$ ratio of the final product is the same as that expected when the effect is ignored. Each sample was analysed on a small length scale using a Philips EM400 TEM with energy dispersive x-ray analysis, indicating that all samples were homogeneous within the resolution of the analysis. We assume, therefore, that any minor inhomogeneity in the precipitate was in any case removed in the grinding and annealing process.

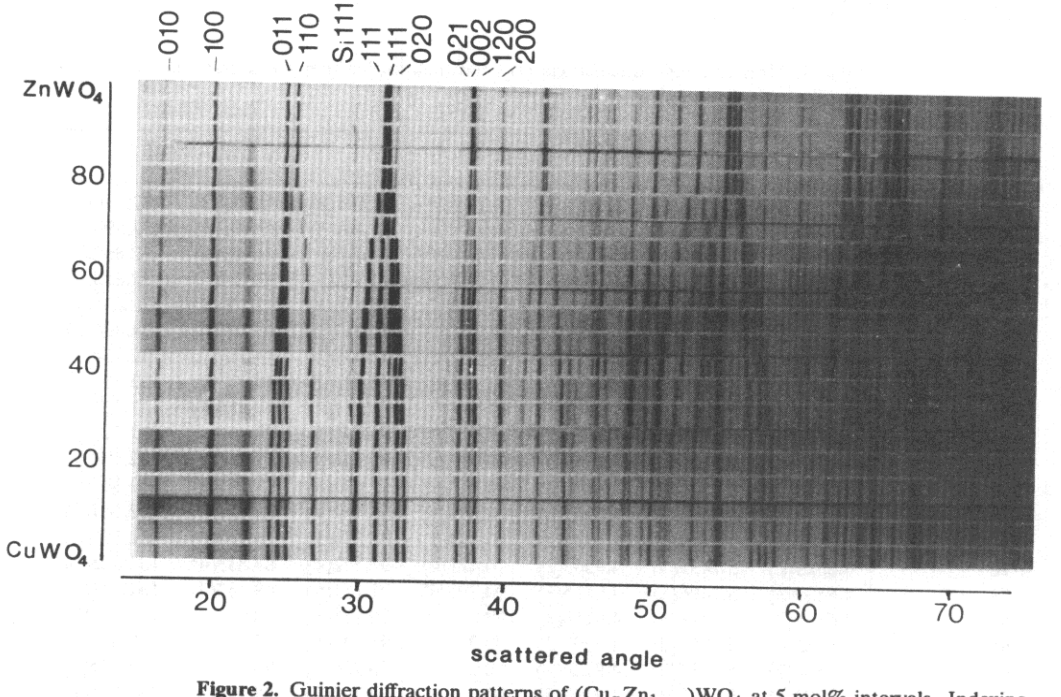

Figure 2. Guinier diffraction patterns of $(Cu_xZn_{1-x})WO_4$ at 5 mol% intervals. Indexing refers to lower-angle lines in the monoclinic phase.

X-ray diffraction patterns of each sample were recorded under ambient conditions on single-sided-emulsion film using a Huber 620 Guinier powder diffraction camera, with Cu $K\alpha_1$ selected from the bent-quartz monochromating crystal. The diffraction patterns further confirmed the homogeneity of the samples and no reflections from potential secondary phases were observed. Samples were mounted on mylar film

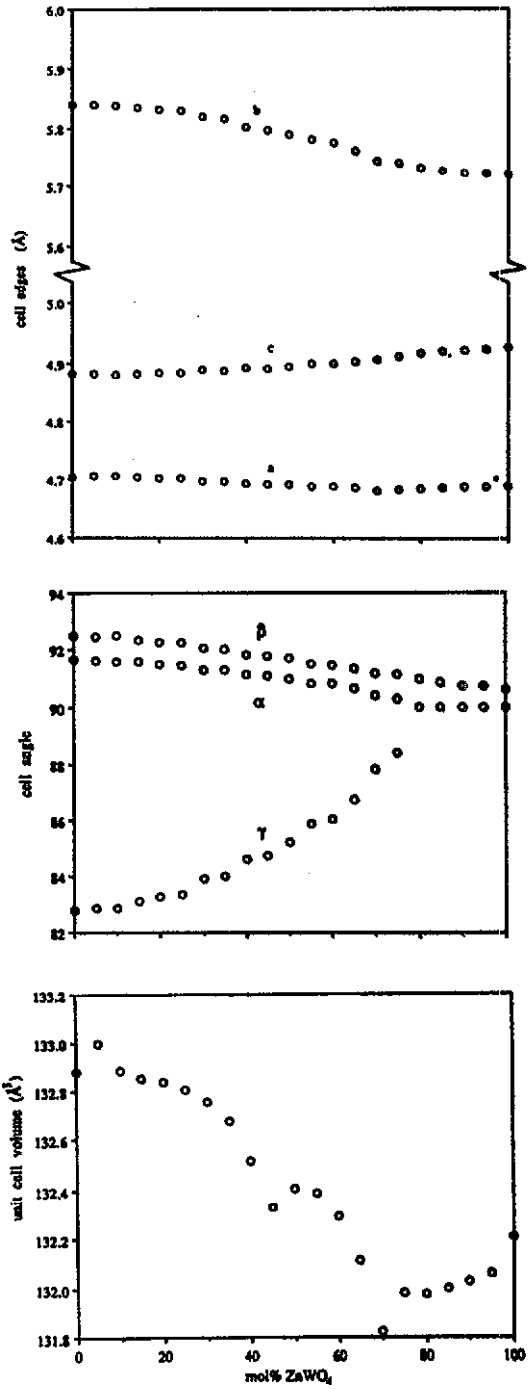

Figure 3. Variation of cell parameters across the solid solution. Data points are greater than the maximum error.

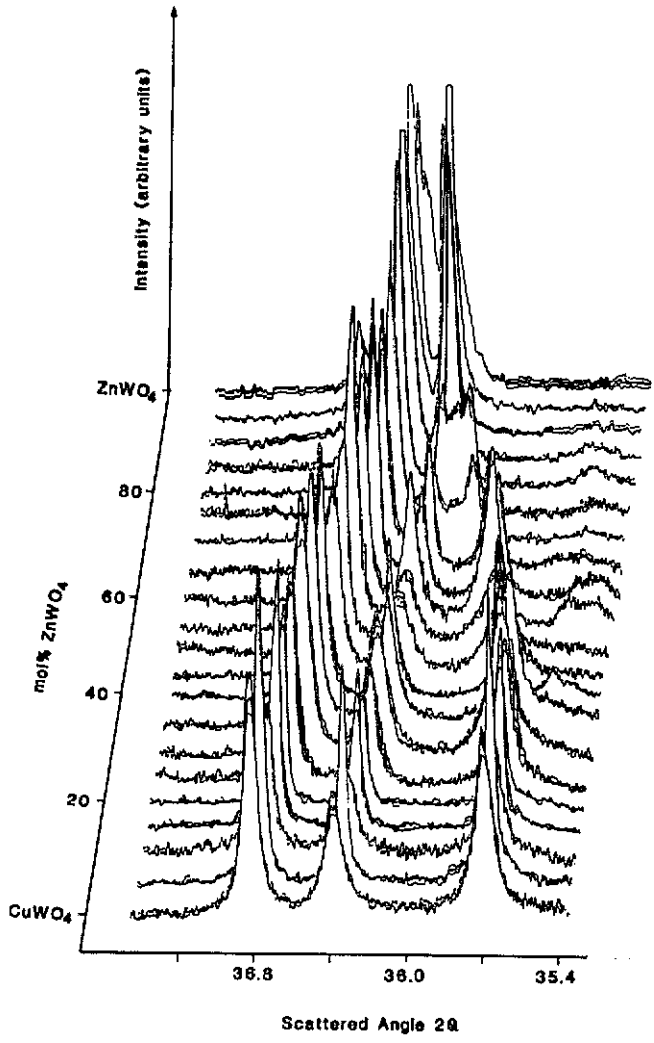

Figure 4. Densitometer traces of powder peaks 002, 021 and $0\bar{2}1$ (left to right) in triclinic $CuWO_4$ which merge as a function of composition to 002 and 021 in monoclinic $ZnWO_4$.

in transmission geometry employing a silicon internal standard. Figure 2 shows the series of room-temperature diffraction patterns recorded at 5 mol% intervals across the composition range.

Peak positions of an average of forty-two Bragg reflections were measured for each sample to a precision of 0.005° 2θ and an accuracy of approximately $\pm 0.001°$ 2θ using a travelling video microscopy system. Film shrinkage and zero-error corrections were made using the positions of the reflections from the internal Si standard. Lattice parameters were calculated by least squares refinement yielding typical standard deviations of one part in 15 000 for both cell edges and for lattice angles. The cell parameters are listed in table 1 and their compositional dependence is shown in figure 3.

4. Results

The most obvious feature of the x-ray powder diffraction patterns is that tungstates in the composition range sanmartinite–cuproscheelite form a complete solid solution at low temperatures. There is no evidence for phase separation at any of the intermediate compositions which we have synthesized. In this respect the low-temperature sub-solidus behaviour is similar to that observed for related wolframite-type binary systems $FeWO_4$–$MnWO_4$ (Buhl and Willgallis 1985), $FeWO_4$–$ZnWO_4$ (Buhl and Willgallis 1986) and $MnWO_4$–$ZnWO_4$ (Buhl and Willgallis 1986).

In contrast to systems previously studied, however, the low-temperature behaviour of the $ZnWO_4$–$CuWO_4$ solid solution is obviously complicated by the change in symmetry from monoclinic to triclinic on increasing Cu content. This results in the splitting of certain monoclinic peaks below 80 mol% $ZnWO_4$ as can been seen in figure 2. The triclinic distortion is, in fact, so great that symmetry related split pairs of peaks quickly separate and overlap one another, giving rise to complicated diffraction patterns at intermediate compositions, which may only be indexed by constant reference to proceeding and preceding patterns in the whole solid solution series.

The compositional dependence of the linewidths of the powder diffraction lines, as measured by a Joyce–Loebl double-beam microdensitometer, is shown by figure 4, demonstrating excellent experimental resolution which corresponds to a linewidth of approximately $0.05°2\theta$. On addition of $ZnWO_4$ a general increase in the linewidth, Γ, of those lines which split in the triclinic phase, for example (021), is seen up to X_c, but these linewidths do not rise to a singularity, as has been observed in As_2O_5 as a function of temperature, by Redfern and Salje (1988). No significant variation in the linewidth, Γ, of the order-paramater-independent Bragg reflections, for example (002), is seen. The widths of the order-parameter-dependent lines in the monoclinic phase are distinctly sharper than in the triclinic phase, however, and this can be attributed to the possible formation of twinned microdomains on the length scale comparable to the correlation of the experiment.

The lattice parameters show a continuous increase in triclinic distortion below approximately 78 mol% $ZnWO_4$ as the α and γ cell angles deviate markedly from 90°. This variation of lattice distortion indicates that the transition to $P\bar{1}$ symmetry as a function of composition is continuous or near-continuous. Other of the lattice parameters also show transition-related changes as a function of composition. The b cell edge shows very slight anomalous increase below about 78 mol% $ZnWO_4$ and a, c and β show barely discernible transition-related changes at the limit of resolution of the experiment. In addition the β cell angle continuously decreases from about 92.5° to about 90.5° with increasing Zn content, indicating a possible trend towards orthorhombic symmetry and the existence of a further phase transition. These observations will now be interpreted within the framework of Landau-type models for ferroelastic and co-elastic phase transitions, employing the concept of spontaneous strain as a measure of the monoclinic–triclinic transition.

5. Spontaneous strain and order-parameter treatment

A properly defined order parameter for the monoclinic-triclinic transition in Cu–Zn tungstates would provide a means of describing its thermodynamic behaviour. For the

moment we define a single-component order parameter, Q, to describe the transition process. Since the triclinic space group is a subgroup of the monoclinic space group and the transition appears continuous (at least as a function of composition, figure 3) then this order parameter can be constructed by application of the Landau rules (e.g. Bruce and Cowley 1981). The order parameter transforms as the active irreducible representation of the supergroup ($P2/c$). The symmetry reduction may be expressed as

$$P2/m = P\bar{1} + c_2 \otimes P\bar{1} \tag{1}$$

where c_2 represents the operaton of the diad. In the transition from the monoclinic $P/2c$ sanmartinite structure to the triclinic $P\bar{1}$ cuproscheelite structure the tungstate unit cell maintains its overall primitive translation periodicity, and the critical point of the Brillouin zone is the origin (Γ point). The loss of the c-glide plane also results in the appearance of superlattice reflections of the type $h0l, l = 2n+1$ in the $P\bar{1}$ phase. This implies an intra-cell displacement pattern of optic character is also associated with the transition, and we can expect optic mode–acoustic mode coupling to the ferroelastic process. The behaviour of certain optic phonons, therefore, be directly coupled to the Γ point behavour, as has been observed in the analogous case of As_2O_5 (Schmahl and Redfern 1988). For the moment we shall ignore the possibility of coupled softening of optic hard modes, although investigations are under way to determine the significance of such phenomena in these tungstates.

The active representation for the Γ point symmetry-breaking process is B_g in point group $2/m$ and so critical lattice vibrations directly related to the order parameter must transform as B_g. One particular consequence of this is that the symmetry-adapted spontaneous strain tensor behaves in the same manner as the order parameter for the transition and is only required to contain strain elements e_{12} and e_{23} (e_6 and e_4 in Voigt notation) in the standard crystallographic setting. From this symmetry analysis we thus predict the onset of spontaneous strain in the triclinic phase with these two components. The strain components may be calculated from the lattice parameters using the result of Redfern and Salje (1987) and choosing a Cartesian coordinate system for the linear Lagrangian spontaneous strain tensor in which

(i) R_2 is parallel to the crystallographic b axis;

(ii) R_3 is parallel to the crystallographic c^* axis; and

(iii) R_1 is perpendicular to both;

from which we obtain:

$$e_{12} = \tfrac{1}{2}e_6 = a(\cos\gamma)/2a_0 \tag{2}$$

$$e_{23} = \tfrac{1}{2}e_4 = \frac{\cos\beta_0}{2\sin\beta_0}\left(\frac{c\cos\alpha}{c_0\cos\beta_0} - \frac{a\cos\gamma}{a_0}\right) \tag{3}$$

where the subscript 0 denotes those parameters expected in the low-symmetry phase by extrapolation of those in the high-symmetry phase to the composition of interest.

It is apparent that a convenient approximation to e_{12} is given more simply by $\cos\gamma$, and this is often taken as a measure of the spontaneous strain for such a monoclinic–triclinic transition. Another commonly employed convenience is the reduction of the second-rank strain tensor into a scalar form to give the amplitude

of the spontaneous strain. This scalar spontaneous strain, ϵ_S, may be defined in a number of ways; Redfern and Salje (1987) chose the simple geometric mean of the Voigt strain tensor elements:

$$\epsilon_s^2 = \sum e_i^2. \tag{4}$$

Figure 5 shows the scalar spontaneous strain, ϵ_S, calculated according to equation (4) for the entire composition range. The magnitude of the spontaneous strain is significantly larger than the majority of elastic transitions, as has already been evinced by the large peak splitting in the diffraction patterns, and amounts to some 6.5% at the $CuWO_4$ end member.

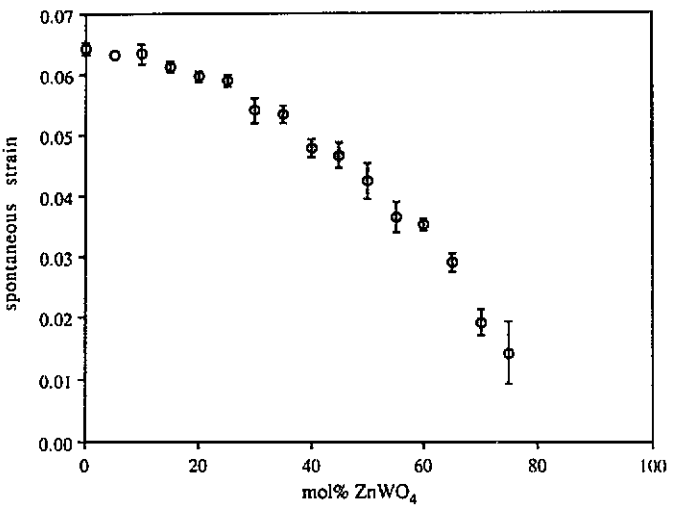

Figure 5. Scalar spontaneous strain, ϵ_s, of $P\bar{1}$ Cu–Zn tungstate as a function of composition

The symmetry change indicates that the transition corresponds to Aizu species $2/mF\bar{1}$ in his nomenclature of ferroelastic phases (Aizu 1970). If the transition is truly ferroelastic this would imply the existence of switchable ferroelastic domains in the triclinic structure, and although twinning has been reported in the $CuWO_4$ end member we have not been able to confirm the existence of twins in our powders of intermediate composition. For the moment we therefore class the transition as *potentially ferroelastic*. We shall now develop a Landau model for the critical behaviour of the spontaneous strain which we observe.

6. Landau model for the transition

Assuming a single uncoupled order parameter for the transition process we first develop a free energy expansion for the structural phase transition between sanmartinite $(P/2c)$ and cuproscheelite $(P\bar{1})$ which accounts for our observations. We may include the spontaneous strain within the excess free energy expression, aware of the fact that the zone-centre character for the phase transition allows linear coupling to

strain in the lowest order (see, e.g. Salje and Devarajan 1986). The expression for a single-order-parameter model following the Landau formalism is thus

$$\Delta F = \tfrac{1}{2}AQ^2 + \tfrac{1}{4}bQ^4 + \tfrac{1}{6}cQ^6 + \lambda_4 Q e_4 + \lambda_6 Q e_6 + \tfrac{1}{2}\sum_{ik} C_{ik} e_i e_k \tag{5}$$

where C_{ik} are the elastic constants and λ_4 and λ_6 are the coupling constants between the order parameter and the spontaneous strain. From this equation we can see that the transition may be driven either by the strain components, e_i, or directly by the order parameter, Q (which we have not yet associated with any particular physical process), or by critical behaviour of the coupling between them (Redfern and Salje 1988).

Equation (5) would usually be applied to a phase transition on increasing temperature by the stipulation that the coefficient of the quadratic term be explicitly temperature dependent $A = a(T - T_c)$ where T_c is the transition temperature. We observe coupling between the spontaneous strain and the solid solution composition, such coupling may be explored by the addition of composition terms into equation (5). It is apparent that the addition of Cu into $ZnWO_4$ stabilizes the low-symmetry structure. For the moment we will assume that the effect of Cu substitution for Zn is equivalent to creating a homogeneous field within the structure. This is valid as long as the Cu concentration is sufficient that the local Ornstein–Zernike strain field associated with each Cu defect ovelap to such an extent that the distance between them is comparable with the hard core of the strain field (Salje 1990). In this case the lowest-order coupling between the molar fraction of $CuWO_4$, x and the order parameter of the triclinic structure Q, is of the form $\zeta x Q^2$ where ζ is the coupling constant (Salje *et al* 1991). The Landau expansion for excess free energy then becomes (ignoring higher-order concentration–order-parameter coupling):

$$\Delta F = \tfrac{1}{2}a(T - T_c)Q^2 + \tfrac{1}{4}bQ^4 + \tfrac{1}{6}cQ^6 + \lambda_4 Q e_4 + \lambda_6 Q e_6 + \sum_{ik} C_{ik} e_i e_k + \zeta x Q^2. \tag{6}$$

In the case of a stress-free crystal $\partial(\Delta F)/\partial e_i = 0$ and hence we obtain

$$e_i = M_i(C_{ik}\lambda_i)Q \tag{7}$$

where M_i are coefficients dependent upon the elastic constants and strain–order-parameter coupling constants. We see that the spontaneous strain is a direct reflection of the order parameter. Thus it follows that the strain coupling terms, elastic energy, and composition-dependent term in equation (6) may all be expressed in terms of the quadratic coefficient of the order parameter in the standard Landau expansion:

$$\Delta F = \tfrac{1}{2}a\left[T - T_c + \left(\sum_{ik} C_{ik} M_i M_k + 2\sum_i \lambda_i M_i\right)/a + 2\frac{\zeta x}{a}\right]Q^2 + \tfrac{1}{4}bQ^4 + \tfrac{1}{6}cQ^6 \tag{8}$$

leading to the renormalized critical temperature:

$$T_c^* = T_c - \left(\sum_{ik} C_{ik} M_i M_k + 2\sum_i \lambda_i M_i\right)/a - 2\frac{\zeta x}{a} \tag{9}$$

which, since the strain and composition interactions are negative and stabilize the low-symmetry structure, leads to an increase in the observed transition temperature.

The expected behaviour of the equilibrium order parameter below the phase transition obviously follows as the well-known result, $Q \propto (T_c^* - T)^\beta$ where $\beta = \frac{1}{2}$ for a second-order transition and $\frac{1}{4}$ for a tricritical transition. Our experiments were carried out under constant conditions of room temperature and pressure; thus if the coefficients of the Landau expansion are independent of composition we obtain (in the case of a second-order phase transition):

$$e_s^2 \propto Q^2 = 2\zeta x/b - \text{constant} = (2\zeta/b)(X_c^* - X) \tag{10}$$

where X_c^* is the observed critical molar proportion $ZnWO_4$ below which the structure transforms to triclinic symmetry at RTP.

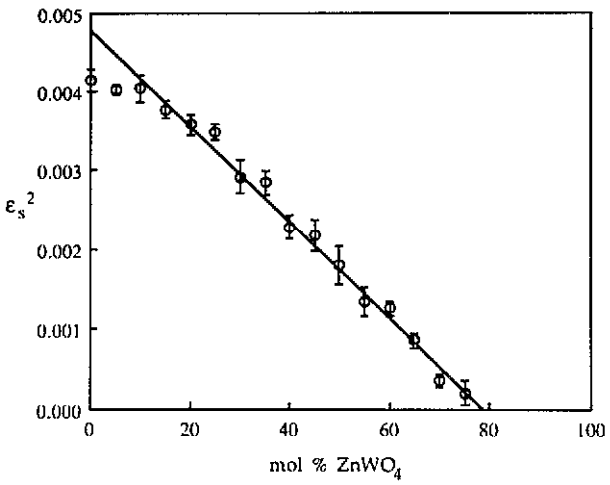

Figure 6. Square of the scalar spontaneous strain in $P\bar{1}$ Cu–Zn tungstate, indicating $Q^2 \propto |X_c^* - X|$, $X_c^* = 0.78$ molar proportion $ZnWO_4$.

Indeed, plotting the square of the spontaneous strain as a function of composition (figure 6) we observe that within the resolution of our experiment the spontaneous strain does indeed behave according to the relation:

$$Q^2 \propto e_s^2 = 0.0048(X_c^* - X)/X_c^* \qquad (X < X_c^*,\ X_c^* = 0.78) \tag{11}$$

which implies that the phase transition is classical second-order Landau in character. The linear relationship shown in figure 6 extends over the entire composition range, indicating again that the ferroelastic phase transition behaviour is essentially mean field in character.

The composition evolution of the individual strain tensor components, e_4 and e_6, as shown in figure 7 yield values for the coupling constants M_4 and M_6 of 0.012 and 0.066 respectively. In addition we find that there is a further spontaneous strain e_{22}. Although such a strain is not predicted from symmetry considerations it reflects a further, as yet unidentified, microscopic process coupled to the $P\bar{1}$–$P2/c$ transition. This additional strain could tentatively be associated with either the excess elongation,

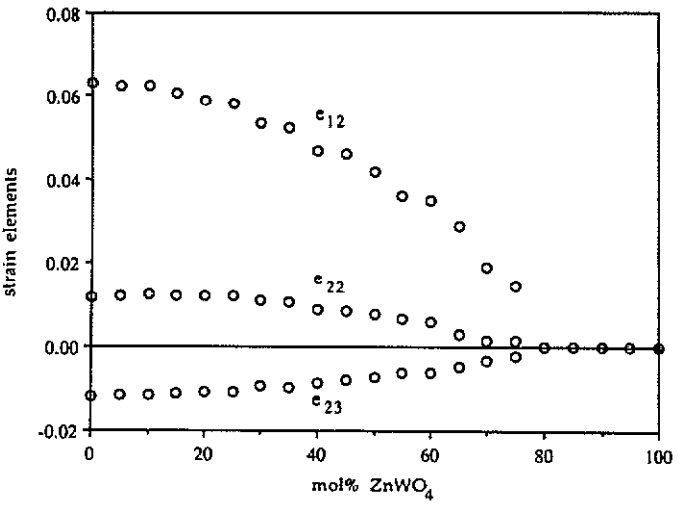

Figure 7. Variation of triclinic strain elements e_{12}, e_{22} and e_{23} as a function of composition.

in the 010 direction, of the CuO_6 octahedra in the structure (associated with Jahn–Teller interaction) or the action of the optic distortion associated with the loss of the c-glide. It acts to induce an excess volume below X_c^* which accounts for the anomolous volume expansion apparent in figure 3. We could, therefore, account for this additional strain by an additional non-symmetry-breaking term, $\sum \Delta V\ Q^2$, in equation (6), with $\Delta V \propto e_{11} + e_{22} + e_{33}$. As such, this contributes substantially to the excess free energy of the low symmetry phase, despite its apparently secondary nature.

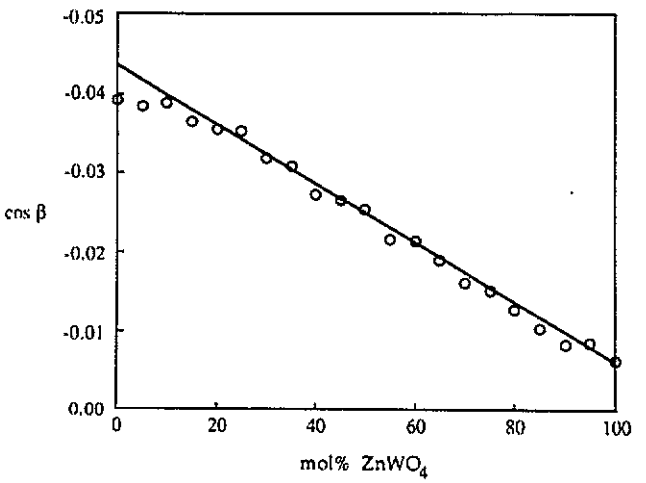

Figure 8. Variation of $\cos\beta$, proportional to e_{13}, in our samples, indicating a continuous trend towards orthorhombic symmetry with increasing Zn content.

Further observation of the lattice parameters reveals the gradual reduction of the β angle across the whole composition range. If this is associated with a further tran-

sition from orthorhombic to monoclinic we can interpret this anomolous behaviour of β in terms of a strain e_{13}, proportional to $\cos\beta$. Plotting $\cos\beta$ as a function of composition we see that the orthorhombic symmetry would appear to become stable at a notional composition of 130 mol% $ZnWO_4$. Figure 8 shows that e_{13} is proportional to composition, if we assume a continuous transition then this behaviour can be understood in terms of e_{13} coupling quadratically to $Q_{\text{ortho-mono}}$, $e_{13} \propto Q^2$, and the transition being a second-order zone boundary transition. This phase is obviously unattainable by compositional variation, but may represent a further $ZnWO_4$ structure stable under different pressure or temperature conditions.

From equation (9) we see that the transition temperature for the $P\bar{1}$–$P2/c$ transition in the Cu–Zn tungstates should be a linear function of composition if the coefficients in the Landau expansion remain constant. We are currently undertaking further investigations into the high-temperature structural states of Cu–Zn tungstates to test the validity of this relationship.

7. Summary

The complete solid solution between $ZnWO_4$ and $CuWO_4$ has been investigated by high-resolution Guinier powder x-ray diffraction. The lattice parameters reveal the existence of a continuous phase transition between the $P2/c$ $ZnWO_4$ sanmartinite structure and the $P\bar{1}$ $CuWO_4$ cuproscheelite structure with a critical composition of $Zn_{0.78}Cu_{0.22}WO_4$. Applying Landau theory, the spontaneous strain is found to behave as the order parameter and amounts to 6.5% in the $CuWO_4$ end member, and a critical exponent $\beta = \frac{1}{2}$, characteristic of classical second-order behaviour, is observed. The structural phase transition is potentially ferroelastic and reflects critical behaviour at the centre of the Brillouin zone. In addition to the symmetry predicted strain tensor components e_{12} and e_{23}, the lattice parameters also reveal the existence of a spontaneous strain component, e_{22}, not required by symmetry. This additional strain, responsible for the anomolous volume expansion, could be associated with either the Jahn–Teller distortion or with the optic distortion associated with the loss of the c-glide and transforms as Q^2.

The lattice parameters also reveal a trend towards orthorhombic symmetry, which would occur at a hypothetical composition of 130 mol% $ZnWO_4$. A strain tensor component e_{13}, proportional to the square of the order parameter indicates that this transition is a second-order zone boundary phase transition.

Acknowledgments

PFS is grateful for the funding of the NERC. SATR acknowledges the support of the Royal Society and the Nuffield Foundation.

References

Aizu K 1970 Determination of the state parameters and formulation of spontaneous strain for ferroelastics *J. Phys. Soc. Japan* **28** 706–16

Arora S K and Mathew T 1989 Dielectric studies of copper tungstate ($CuWO_4$) crystals *Phys. Status Solidi* A **116** 405–13

Arora S K, Mathew T and Batra N M 1988 Growth and important properties of $CuWO_4$ single crystals *J. Cryst. Growth* **88** 379–82

—— 1989 Optical characterization of $CuWO_4$ single crystals *J. Phys. Chem. Solids* **50** 665–8

Basu A K and Sale F R 1978 Copper–tungsten composite powders by the hydrogen reduction of copper tungstate *J. Mater. Sci.* **13** 2703–11

—— 1979 The controlled reduction of copper tungstate in H_2O/H_2 mixtures *J. Mater. Sci.* **13** 91–9

Bharati R, Shanker R and Singh R A 1980 Electrical transport properties of copper (II) tungstate ($CuWO_4$) *Pramana* **14** 449–54

Broch E K 1929 Unterschungen über Kristallstrukturen des Wolframittypus und des Scheelittypus *Norsk Akad., Oslo, Mater.-Nat. Kl. Skrifter* **8** 4–61

Bruce A D and Cowley R A 1981 *Structural Phase Transitions* (London: Taylor and Francis)

Buhl J C and Willgallis A 1985 On the hydrothermal synthesis of wolframite *J. Chem. Soc.* **48** 93–102

—— 1986 The low temperature crystallization of $(Fe,Mn)WO_4$ wolframite, $(Zn,Fe)WO_4$ sanmartinite and $(Zn,Mn)WO_4$ solid solutions under hydrothermal conditions *Chem. Geol.* **56** 271–9

Chicagov A P, Ilyukhin V V and Belov N V 1966 Crystal structure of $CdWO_4$ *Sov. Phys.–Dokl.* **11** 11–3

Cid-dresdner H and Escobar C 1968 The crystal structure of ferberite, $FeWO_4$ *Z. Kristallogr.* **127** 61–7

Dachs H, Stoll E and Weitzel H 1967 Kristallstruktur und Magnetische Ordnung des Hubnerits, $MnWO_4$ *Z. Kristallogr.* **125** 120–9

Filipenko O S, Pobedimskay E A and Belov N V 1968 Crystal structure of $ZnWO_4$ *Sov. Phys.–Crystallogr.* **13** 127–9

Földvári I, Capelletti R, Kappers L A, Gilliam O R and Watterich A 1989 The role of OH^- ions in the charge compensation of impurities in $ZnWO_4$ single crystals *Phys. Lett* **135A** 363–7

Földvári I, Péter A, Keszthelyi-Lándori S, Capelletti R, Cravero I and Schmidt F 1986 Improvement in the quality of $ZnWO_4$ single crystals for scintillation applications *J. Cryst. Growth* **79** 714–9

Keeling R O 1957 The structure of $NiWO_4$ *Acta Crystallogr.* **10** 209–13

Kihlborg L and Gebert E 1970 $CuWO_4$ a distorted wolframite-type structure *Acta Crystallogr.* B **26** 1020–5

Pisorevskii Y V, Sil'vestrova I M, Voszka R, Péter A, Földvári I and Janszky J 1988 Elastic and acoustic properties of zinc tungstate ($ZnWO_4$) single crystals *Phys. Status Solidi* A **107** 161–4

Redfern S A T and Salje E 1987 Thermodynamics of plagioclase II: Temperature evolution of the spontaneous strain at the $I\bar{1}$-$P\bar{1}$ phase transition in anorthite *Phys. Chem. Minerals* **14** 189–95

—— 1988 Spontaneous strain and the ferroelastic phase transition in As_2O_5 *J. Phys. C: Solid State Phys.* **21** 277–85

Salje E 1990 *Phase Transitions in Ferroelastic and Co-elastic Crystals* (Cambridge: Cambridge University Press)

Salje E, Bismayer U, Wruck B and Hensler J 1991 Influence of lattice imperfections on the transition temperature of structural phase transition: the plateau effect *Phase Transitions* **35** 61–74

Salje E and Devarajan V 1986 Phase transitions in systems with strain-induced coupling between two order parameters *Phase Transitions* **6** 235–48

Schmahl W W and Redfern S A T 1988 An x-ray study of coupling between acoustic and optic modes at the ferroelastic phase transition in As_2O_5 *J. Phys. C: Solid State Phys.* **21** 3719–25

Scott J F 1968 Dipole–dipole interactions in tungstates *J. Chem. Phys.* **49** 98–100

Shoji T and Sasaki N 1978 Fluorescent colour and x-ray powder data of synthesized scheelite–powellite series as guides to determine its composition *Mining Geology* **28** 397–404

Sleight A W 1972 Accurate cell dimensions for ABO_4 molybdates and tungstates *Acta Crystallogr.* B **28** 2899–902

Šroubek Z and Žďánský K 1966 Electron spin resonance of Cu^{2+} ion in $CdWO_4$, $ZnWO_4$ and $MgWO_4$ single crystals *J. Chem. Phys.* **44** 3078–83

Tyson R M, Hemphill W R and Theisen A F 1988 Effect of W:Mo ratio on the shift and excitation spectra in the scheelite-powellite series *Am. Mineral.* **73** 1145–54

Ülkü D 1967 Unterschungen zur Kristallstructur und Magnetischen Struktur des Ferberits, $FeWO_4$ *Z. Kristallogr.* **124** 192–219

Van Uitert L G, Rubin J J and Bonner W A 1963 Preparation of single crystals of molybdates and tungstates of a number of divalent metal ions *J. Am. Ceram. Soc.* **46** 512

Von Klein S and Weitzel H 1975 PERNOD - ein Programm zur von Kristallstructurparameterrn aus Neutronenbeugungspulverdiagrammen *J. Appl. Crystallogr.* **8** 54–9

Watterich A, Edwards G J, Gilliam O R, Kappers L A, Madacsi D P, Raksányi K and Voszka R 1991 ESR of platinum impurity ions in $ZnWO_4$ single crystals *J. Phys. Chem. Solids* **52** 449–55